

844. A quantitative study of the blade passing frequency noise of a centrifugal fan

Jian-Cheng Cai¹, Da-Tong Qi²

¹College of Engineering, Zhejiang Normal University, Jinhua, 321004, China

²School of Energy and Power Engineering, Xi'an Jiaotong University, Xi'an, 710049, China

E-mail: ¹763421532@qq.com, ²dtqi@mail.xjtu.edu.cn

(Received 8 Jun 2012; accepted 4 September 2012)

Abstract. Tonal noise constitutes the major part of the overall fan noise, particularly the blade passing frequency (BPF) noise, which is generally the most annoying component. This paper quantitatively studies the BPF tonal noise of a centrifugal fan, including casing aerodynamic noise, blade aerodynamic noise and casing structural noise. Firstly, fan noise generation and propagation is discussed and the measured spectra of fan noise and casing vibration are presented. Secondly, a fully 3-D transient simulation of the internal flow field of the fan is performed. Flow interactions between the impeller and the volute casing result in the periodic pressure fluctuations on solid walls of the impeller and casing. This pressure fluctuation, in the aeroacoustic study, is modeled as aeroacoustic dipole source according to the Lighthill's acoustic analogy theory. With the inhomogeneous wave equations solved by the boundary element method, the BPF casing and blade aerodynamic noise radiation is obtained. Finally, in the casing structural noise study, the casing structural vibration under the excitation of BPF pressure fluctuation is calculated by the finite element method and sound radiation is solved by the boundary element method subsequently. Results demonstrate that the casing aerodynamic noise is the main contribution to the centrifugal fan noise with the sound power level of 103 dB followed by the blade noise (91 dB), and the casing structural noise is 79 dB.

Keywords: centrifugal fan, unsteady flow field, blade passing frequency, aerodynamic noise, structural noise.

Introduction

As a type of turbomachinery, centrifugal fans are widely employed for industrial and civilian use because they achieve high pressure ratios in a short axial distance compared to axial fans. However, the noise generated by centrifugal fans can become a serious problem. According to the spectrum characteristics of fan noise, it can be divided into discrete tonal noise, induced by the periodic interactions between the rotating impeller and the volute casing especially the volute tongue, and a broadband noise, mainly due to the turbulent flow fluctuations in the inlet stream, in boundary layer, and wake behind the blade. The blade passing frequency noise is in general the most notable and annoying component [1-3]. According to the noise generation mechanism, fan noise can be classified into aerodynamic noise generated by turbulent flow fields directly and vibroacoustic noise caused by structural vibration. Jeon [4] points out that in the case of large-sized fan, the levels of the vibration-induced noise and the flow-induced noise are comparable, but in the case of small and the middle-sized fans, the flow-induced noise is dominant.

The internal turbulent flow is the root cause of fan noise: on the one hand, it generates aerodynamic noise as the aeroacoustic source; on the other hand, it induces structural vibration and generates vibration-induced noise. Mechanical excitations such as unbalanced rotors, vibration of motors, defected bearings can cause fan structural vibration as well. In this study, the flow-induced vibration is considered. Therefore, for a reliable prediction of fan noise, precise analysis of flow field is essential. The capability of the existing computers allow the numerical simulation of complex flow features that commonly take place in centrifugal fans: unsteady turbulent flow, important 3-D effects and complex configurations. Nowadays, some commercial CFD packages, showing their validity and reliability for the description and prediction of the

unsteady flow in turbomachinery, are available, and good agreements between the CFD and experiment results of the investigation of flow fields in centrifugal fans have been found [1, 5-7].

As for the numerical prediction of aerodynamic noise, there are two approaches, namely the direct computation and indirect or hybrid computation [8]. The direct approach computes the sound together with its fluid dynamic source field by solving the compressible flow equations. The hybrid approach takes into account the difference of the temporal and spatial scales between the flow field and the acoustic field. This consideration allows a segregation of the complete problem of both generation and propagation of the aerodynamic noise into two separate problems: 1) the acoustic sources and the flow field are determined firstly, and 2) the calculation of the acoustic field is completed as a direct consequence of those sources. The direct approach is basically used in problems of computational aeroacoustics; it requires extremely high computational resources if an accuracy is desired for the resolution (for both calculation efforts and time necessary to achieve a complete solution of the flow and acoustic fields). At present, the complexity of the 3-D phenomena involved in any turbomachine is far beyond the scope of this approach [9]. There are several hybrid approaches [10, 11], of which the most widely used is the CFD plus acoustic analogy method.

Lighthill's acoustic analogy theory recasts the compressible fluid dynamic equations into an inhomogeneous wave equation to predict sound radiated by an unsteady flow in an unbounded region [12]. It was generalized by Ffowes Williams and Hawkings [13] to include the presence of foreign bodies. Let the foreign body is closed by the surface defined by $f(\mathbf{x}, t) = 0$, with $f < 0$ in the interior, $f > 0$ outside, and such that the outward unit normal vector $\mathbf{n} = \nabla f$. The FW-H equation is given as follows:

$$\frac{1}{c^2} \frac{\partial^2 p'}{\partial t^2} - \nabla^2 p' = \frac{\partial}{\partial t} [\rho_0 v_n \delta(f)] - \frac{\partial}{\partial x_i} [P_{ij} n_j \delta(f)] + \frac{\partial^2}{\partial x_i \partial x_j} [T_{ij} H(f)] \quad (1)$$

where c is the speed of sound, p' the far field sound pressure ($p' = p - p_0$) and t denotes time. $\delta(f)$, and $H(f)$ represent the Dirac delta function and Heaviside function with $\delta(f) = H'(f)$. v_n is normal velocity of the control surface. ρ_0 is the ambient fluid density. $P_{ij} = -p' \delta_{ij} + \tau_{ij}$, and $T_{ij} = \rho v_i v_j + (p' - c^2 \rho') \delta_{ij} - \tau_{ij}$ are the fluid stress tensor, and Lighthill's stress tensor, respectively. The first term in the right hand of Eq. (1) is the monopole source, known as the thickness noise; it represents a surface determined by the kinematics of body. The second term is also corresponding to a surface distribution, which comes from interaction between the flow and the moving bodies. This source term is usually known as loading noise, with dipolar directivity (dipole source). The third source term represents a volume distribution that corresponds to the Lighthill's stress tensor with a quadrapolar character.

A fundamental assumption for acoustic analogy-based hybrid prediction is the one-way coupling of flow and sound. In other words, the unsteady flow generates sound and its propagation; while the sound waves do not significantly affect the flow. The principal application of the hybrid approach lies in flows with low Mach numbers; at sufficient low Mach numbers (< 0.3), incompressible flow solutions can be adequate for approximating acoustic source terms [8, 14].

Many authors use the hybrid method to predict fan noise [1, 4, 6, 15, 16]: unsteady flow fields are simulated by CFD technique either use LES or Reynolds averaged Navier-Stokes equations (RANS) approach; aeroacoustic sources are determined according to the FW-H equation, and sound pressure values at specific locations are obtained by integrating the FW-H equation with respect to time. Sound sources directly radiating noise into free space is inherently assumed in this methodology; the scattering effect of fan casing is not considered. In mathematic

terms, this approach only solves the particular solution of the corresponding inhomogeneous wave equation. This ignorance may cause some differences in the noise level prediction comparing the measured results [9]. Jeon [4] points out that to a centrifugal fan, which has volute casing, the scattering effect must be considered in order to compare the predicted sound pressure level (SPL) to the measured one. Actually, the propagation of the internal aerodynamic noise of a centrifugal fan is as follow: it mainly propagates along the volute housing and pipes if the fan is installed in a pipeline system, and at the inlet/outlet it emits to the environment; on the other side, the internal sound waves excite the casing and pipes to vibrate and thus transmit to the environment, i.e., they penetrate the casing and pipe walls. Of the acoustic sources of centrifugal fans and pumps, studies show that the dominant acoustic source is the dipole source [16-19]; in the case of high Reynolds number flow as encountered in the fan internal flow, $P_{ij}n_j \approx -p'n_i$ representing the pressure loading exerted by the solid body on the fluid.

The aforementioned studies about fan noise mostly deal with the aerodynamic noise; very limited work has been made on the structural noise. To the authors' knowledge, there is no work systematically studying different fan noise constitutions. This paper quantitatively studies the blade passing frequency (BPF) noise of a centrifugal fan. Fully transient 3-D turbulent flow was obtained firstly through CFD approach. According to FW-H equation, the surface pressure over the casing and blade surface was regarded as aeroacoustic dipole source. The calculation of casing BPF aeroacoustic noise was straightforward, while the blade noise is tricky due to the blade rotation. We used the Loswon's formulation of rotor noise model based on the reformulation of moving source FW-H equation in the frequency domain. The full solution of the inhomogeneous wave equation was obtained by BEM with the combination of the particular solution (the incident sound) and the general solution (the scattering sound); this approach can take the casing scattering effect into account in simulating the sound propagation. The fan casing structure vibration and sound radiation under the aerodynamic pressure excitation was studied using the fluid-structure-sound one way coupling methodology. Studying fan structural noise has the significance: in some cases where turbomachines are installed in pipelines, for example, fans in HVAC, and centrifugal pumps, compressors, so that the direct emission of the internal aerodynamic noise is blocked off. The noise radiation is ascribed to structural vibration.

The Centrifugal Fan - Its Noise and Vibration Characteristics

The centrifugal fan under study is driven by an AC 3.0 kW motor rotating at the speed $N = 2900$ rpm. The shrouded impeller has $B = 12$ forward-curved blades with the outlet diameter $d = 400$ mm and a vaneless diffuser ($d_2 = 400$ mm). The blades are made of flat sheet metal. The rotational frequency (RF) is $N/60 = 48.3$ Hz, and the blade passing frequency (BPF) is $B \times \text{RF} = 580$ Hz. The volute housing collects the air flow leaving from the impeller so that air flow can pass through the fan discharge duct. The minimum distance between the impeller and the volute tongue, namely the cutoff clearance, is 10 mm. The main dimensions of the fan are shown in Fig. 1.

A standard test facility for the aerodynamic performance and noise characteristics of the investigated fan was made in a hemi-anechoic chamber according to China Standard GB/T-1236-2000: Industrial fans performance testing using standardized airways, and GB/T 2888-91: Methods of noise measurement for fans, blowers, compressors and roots blowers. Fig. 2 shows the sketch of the test facility with its main elements. Detailed technical parameters of the test equipment can found in [20].

At the inlet of the duct, a regulation devise is used to control the flow rate. The performance dimensionless curves are illustrated in Fig. 3, with the flow coefficient defined by $\phi = Q / (d^2 u_2 \pi / 4)$, where Q is the volumetric flow rate, d the outlet diameter of the impeller and u_2 the tip circumferential velocity at impeller outlet defined by $u_2 = 2\pi N / 60 \times d / 2$. Total

section, a fully 3-D unsteady turbulent flow on the whole impeller-volute configuration was calculated using the computational fluid dynamics method.

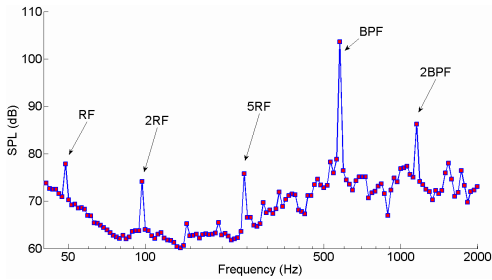


Fig. 4. Sound pressure spectrum of fan noise

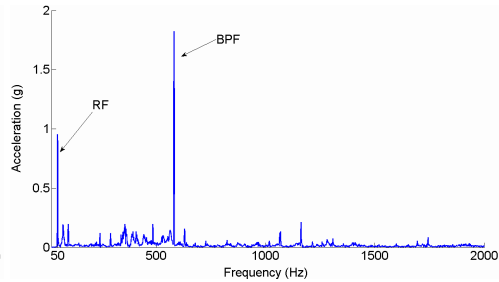


Fig. 5. Casing vibration spectrum

Unsteady Viscous Flow Computation

CFD technology has been proven to be a very useful tool in the analysis of the complex flow of turbomachinery both in design and performance prediction, and widely employed in simulating the fully 3-D unsteady flow in centrifugal turbomachinery. It can provide detailed flow information which is difficult or impossible to obtain through experimental measurements. In this study, 3-D numerical simulation of the complete unsteady flow on the whole impeller-volute configuration was carried out using the commercial CFD package ANSYS CFX[®], which uses the finite volume method and solves the Navier-Stokes equations on unstructured meshes.

The characteristic flow Mach number described by the blade tip circumferential velocity is $u_2/c = 0.179$ (<0.3), therefore the flow was assumed to be incompressible. Due to the low pressure rise, we further regarded the flow as isothermal. Thus, the continuity equation and the momentum equation could be solved independent of the energy equation. The characteristic Reynolds number depicted by the blade tip circumferential velocity and the impeller blade outlet diameter was 1.57×10^6 , indicating the internal flow was turbulent in nature. It was appropriate to solve the unsteady Reynolds averaged Navier-Stokes equations (URANS) economically without loss of resolving the main characteristics of flow fields such as mean pressure fluctuations. URANS are obtained by representing a flow property, e.g., velocity and pressure, in the Navier-Stokes equations as the sum of a steady mean component and a time-varying fluctuating component with zero mean value. As a result six additional unknowns, namely, the Reynolds stresses, are introduced in the time averaged momentum equations. Turbulence modeling procedures are of sufficient accuracy and generality to predict the Reynolds stresses. In the present simulation, standard $k-\epsilon$ model was adopted to depict the turbulence characteristics of the internal flow. The scalable wall-function was used to describe the near wall velocity. The $k-\epsilon$ model is well established and the most widely validated turbulence model; it gives excellent performance for many industrially relevant flows [21]. It should be pointed out that solving unsteady RANS together with turbulence model could provide adequate unsteady flow information to predict the tonal noise of fans, but Large Eddy Simulation (LES) should be employed when predicting broadband noise [22, 23].

The mesh system of a fan was divided into the inlet (pipe), impeller, and outlet (volute) regions; the inlet and outlet regions are in the stationary coordinate system and the impeller region is generally described in the rotational coordinate system. The axial gap between the impeller and the volute casing was modeled regarding its importance in the excitation of casing vibration. Khelladi et al. [24] studied the flow field of a centrifugal fan with and without taking into account the axial gap, and found that the numerical pressure rise taking into account the axial gap was in good agreement with the experimental results, particularly, at large flow rates. Hexahedral cells were used to define the flow region of the centrifugal fan. Though the

hexahedral mesh requires more effort than the tetra mesh, it pays off by the fact that fewer hexahedral elements are required than tetrahedral elements to resolve physics for most CFD applications. A mesh independence test was firstly performed to identify the optimal mesh system. Results indicate that when the total element number is over 0.6 million, the overall aerodynamic performance, i.e. the total pressure and efficiency, reaches an asymptotic value as the number of meshes increases, while regarding the pressure distribution over the casing surface it shows that a mesh system over 1.1 million cells is sufficiently reliable to ensure mesh independence [25]. The final mesh system of 1.6 million cells was adopted. Fig. 6 shows two mesh sections at the middle span of the volute and the meridian plane.

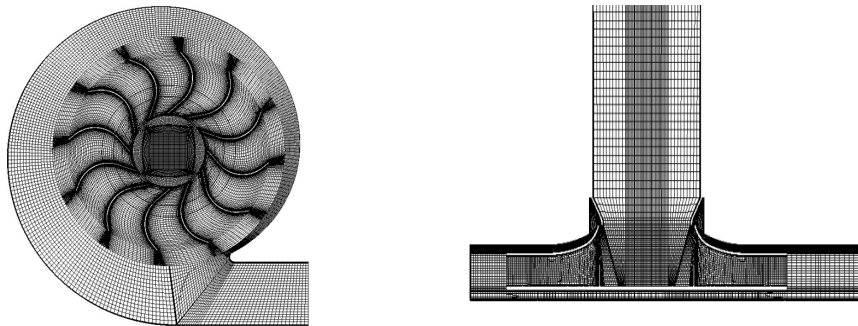


Fig. 6. Mesh used in CFD

A steady simulation using the frozen-rotor approach was firstly performed. In this case, the relative position of the impeller and the volute casing didn't change during the calculation. The iterating residual was set to less than 1.0^{-5} , which is a good convergence and usually sufficient for most engineering applications according to the ANSYS CFX-Solver Modeling Guide. The calculated fan performance is plotted in Fig. 3. Comparing with the experimental results, a good agreement was found demonstrating the reliability of CFD simulation. Fig. 7 provides the static pressure distribution over the blade and casing surfaces. One can observe that pressure increases along the radial direction outward, and the pressure field over the volute tongue is rather complicated. Two pressure monitoring points were set on the blade and the volute tongue indicated by the arrows in Fig. 7, to observe the characteristics of pressure fluctuation in the following unsteady simulation.

The results of the steady simulation served as the initial condition for the unsteady calculation. In unsteady simulation, the sliding mesh technique was applied to the interfaces in order to allow the unsteady interactions between the impeller and the volute, i.e., the meshes change their relative positions during the calculation according to the angular velocity of the impeller. A complete impeller revolution was divided into 512 time steps, i.e., each time step spans $60/2900/512 = 4.041 \times 10^{-5}$ s. The chosen time step was related to the rotational speed of the impeller and was sufficiently small to provide time resolution of pressure fluctuations. After several impeller revolutions, the computation became stable and the temporal data were saved at each time step. A total of 2048 time steps, i.e., 4 revolutions, were sampled.

The pressure fluctuations at the two monitoring points are presented in Fig. 8. The pattern of pressure fluctuation at the volute tongue is very regular: the volute tongue suffers 12 fluctuations in one impeller revolution, i.e., as each blade passage is passing by, the volute tongue perceives an impulse since the pressure side of the blade has the higher pressure and velocity than the suction side. In other words, the BPF component of the volute tongue pressure fluctuation is obvious, and we can conclude the BPF component is outstanding in the frequency spectrum. Of the blade pressure fluctuation, it is interesting to find there are only four peaks and troughs in one impeller revolution, i.e., as the blade revolves, it suffers 4 major pressure fluctuations. This may be ascribed to the existence of the volute casing: the volute profile consists of 4 different

arcs with different center and radius, see Fig. 1. Since the flow is subsonic, the downstream volute casing has the back reaction to the impeller. Particularly when the blade sweeps over the volute tongue where the pressure field varies vehemently, intense pressure fluctuation occurs.

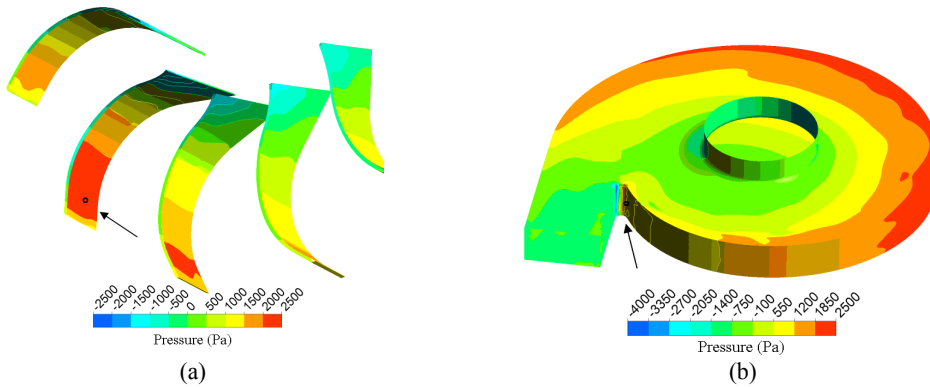


Fig. 7. Static pressure distribution: (a) blade; (b) volute casing

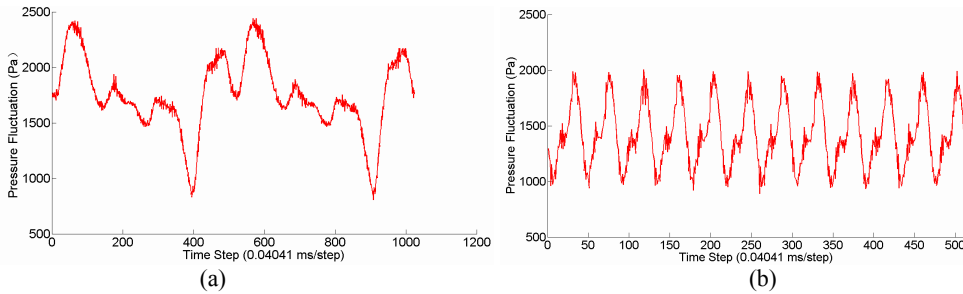


Fig. 8. Pressure fluctuations at the monitoring points: (a) blade; (b) volute tongue

Fig. 9 shows the instantaneous velocity vectors around the volute tongue at the volute middle span; velocity vectors in the impeller is viewed by an observer attached to the impeller, while the velocity vectors in the volute is the absolute velocity viewed in a fixed frame. The wake around the blade trailing edge at the suction side where vortex shedding occurs is obvious. These wakes are believed to introduce mixing losses and cause unsteady flow, resulting in noise, inefficiency, and vibration [26]. As the impeller rotates, the conferral non-uniform flow pattern influences the downstream volute casing and cause pressure fluctuations on it.

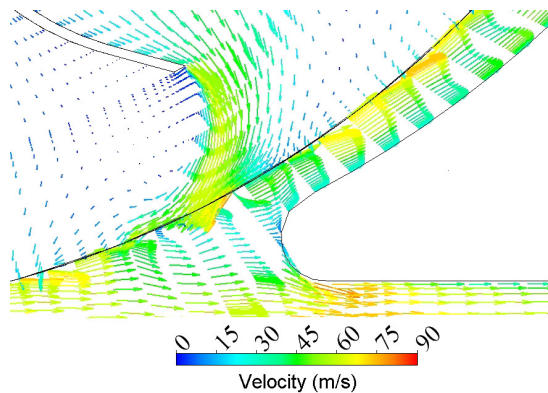


Fig. 9. Instantaneous velocity vectors at the middle span

Prediction of Tonal BPF Aerodynamic Noise

Lighthill's acoustic analogy theory is employed to quantitatively predict the blade and casing BPF aerodynamic noise. The noise due to the aerodynamic forces applied on the surfaces of the casing and blades is dominant compared to other type noise sources in the case of subsonic flow fans. For this reason only the dipole source is considered in this study. With the aeroacoustic source, an inhomogeneous wave equation is obtained. The solution of inhomogeneous wave equation consists of a special solution and the general solution of the related homogeneous wave equation; the special solution represents the incident sound pressure p_{inc} of the source, i.e., the sound wave radiated into free space, and the general solution represents the scattered sound pressure field p_{sca} due to the scattering from objects. The total pressure $p_{tot} = p_{inc} + p_{sca}$ satisfies both the wave equation, including the source terms, and the boundary conditions.

Denoting the incident pressure and incident normal velocity on the mesh by p_{inc} and v_{ninc} , they are satisfying the inhomogeneous wave equation:

$$(\nabla^2 + k^2)p'_{inc} = Q(\mathbf{r}_s) \quad \text{in the domain} \quad (2)$$

On the other hand, by definition of v_{ninc} , we have:

$$\partial p'_{inc} / \partial n = -i\rho_0\omega v_{ninc} \quad \text{on the boundary} \quad (3)$$

The following homogeneous problem, i.e., without sources, is then solved to obtain the scattered pressure p_{sca} :

$$(\nabla^2 + k^2)p'_{sca} = 0 \quad \text{in the domain} \quad (4)$$

$$\partial p'_{inc} / \partial n = -i\rho_0\omega v_{nsca} = i\rho_0\omega v_{ninc} \quad \text{on the boundary} \quad (5)$$

Because of the linearity of the equations and of the boundary conditions, it is clear the total pressure $p_{tot} = p_{inc} + p_{sca}$ satisfies:

$$(\nabla^2 + k^2)p'_{tot} = Q(\mathbf{r}_s) \quad \text{in the domain} \quad (6)$$

$$\partial p'_{inc} / \partial n = 0 \quad \text{on the boundary} \quad (7)$$

In this study we use the strategy mentioned above to solve the blade and casing BPF aerodynamic noise. The casing structure is assumed to be rigid such that the normal velocity vanishes on its surface. The calculation of the casing noise is straightforward because the casing is stationary. In this case, the FW-H equation (Eq. (1)) is reduced into Curle's equation [27], and the inhomogeneous Helmholtz equation is obtained after Fourier transform:

$$(\nabla^2 + k^2)p' = \frac{\partial}{\partial x_i} ((p - p_0)n_i \delta(f)) \quad (8)$$

where $(p - p_0)n_i$ is the aerodynamic force exerted on the casing surface. The incident field can be obtained using the free-field Green function $G(\mathbf{r}_o, \mathbf{r}_s)$ of the frequency-domain wave equation conveniently:

$$p'_{inc}(\mathbf{r}_o) = \iint_S (p_0 - p) \partial G / \partial n dS(\mathbf{r}_s) \quad (9)$$

The calculation of blade noise is tricky due to the rotation of the blade; here we use the Lawson's rotor noise model which is based on the FW-H equation of moving dipole source. The time-domain solution to FW-H equation with only the moving dipole source is given by:

$$p'_{inc}(\mathbf{r}_o, t) = -\frac{1}{4\pi} \iint_S \frac{r_i}{cDr^2} \frac{\partial}{\partial \tau} \left(\frac{F_i}{D} \right) dS \quad (10)$$

where $\tau = t - r/c$ is the retarded time, and $D = |1 - M_r|$ is the Doppler amplification factor due to the moving source (in the relative reference frame) with $M_r = \mathbf{M} \cdot \mathbf{r} / r$ (Mach number of the

sources in the direction of observing point). F_i is the force component in the i -direction exerted by the body on the fluid. The reference of the impeller used to derive the Lawson's formula is illustrated in Fig. 10. The dipole source \mathbf{F} rotates around \bar{e}_3 with an angular velocity ω , and is assumed to be periodic with the rotational period $2\pi/\omega$; therefore it can be expanded into Fourier series with the m th Fourier coefficient given by:

$$\mathbf{F}(m) = \frac{\omega}{2\pi} \int_0^{2\pi/\omega} \mathbf{F}(t) e^{im\omega t} dt \quad (11)$$

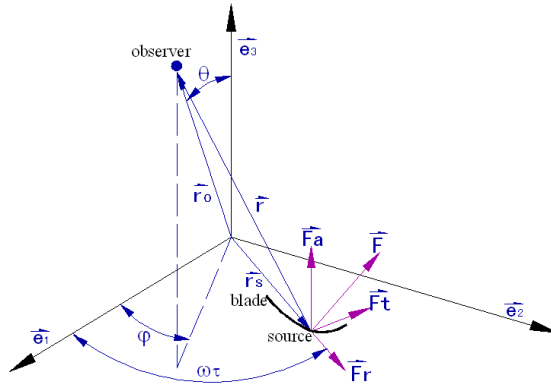


Fig. 10. Reference of the impeller

Fourier transform and integration by parts of Eq. (10) gives:

$$p'_{inc}(\mathbf{r}_o, m) = \frac{im\omega^2}{8\pi^2 c} \iint_S \int_0^{2\pi/\omega} \frac{r_i F_i}{r^2} e^{im\omega(\tau+r/c)} d\tau dS \quad (12)$$

\mathbf{F} can be decomposed into radial, tangential and axial components (F_r, F_t, F_a). The distance between the source and the observer is given by:

$$\mathbf{r} = \begin{pmatrix} r_o \sin(\theta) \cos(\phi) - r_s \cos(\omega\tau) \\ r_o \sin(\theta) \sin(\phi) - r_s \sin(\omega\tau) \\ r_o \cos(\theta) \end{pmatrix} = \begin{pmatrix} r_1 \\ r_2 \\ r_3 \end{pmatrix} \quad (13)$$

For each element dS of the blade surface, a force \mathbf{F} is applied, it is defined by:

$$\mathbf{F} = \begin{pmatrix} F_r \cos(\omega\tau) + F_t \sin(\omega\tau) \\ F_r \sin(\omega\tau) - F_t \cos(\omega\tau) \\ F_a \end{pmatrix} = \begin{pmatrix} F_1 \\ F_2 \\ F_3 \end{pmatrix} \quad (14)$$

Substituting Eqs. (13) and (14) into Eq. (12), and using the following generating function (Jacobi-Anger Expansion):

$$e^{-iz \cos \beta} = \sum_{m=-\infty}^{\infty} (-i)^m m J_m(z) e^{-im\beta} \quad (15)$$

($J_m(z)$ is the Bessel function of the first kind.), the sound pressure at the n th harmonic produced by an impeller with B identical equally spaced blades is finally obtained:

$$p'_{inc}(\mathbf{r}_o, nB) = \frac{inB^2\omega}{4\pi cr_o} e^{in\omega B(r_o/c)} \iint_S \sum_{m=-\infty}^{\infty} e^{i(nB-m)(\phi-\pi/2)} \times \{i \sin \theta J'_{nB-m}(k_n r_s \sin \theta) F_r(m) + [\cos \theta F_a(m) - \frac{nB-m}{nBM_{rs}} F_t(m)] J_{nB-m}(k_n r_s \sin \theta)\} dS \quad (16)$$

where $k_n \equiv n\omega/c$ is the n th harmonic of the rotational frequency, $(F_r(m), F_t(m), F_a(m))$ is the m th Fourier coefficients of (F_r, F_t, F_a) determined by Eq. (11) and $M_{rs} = r_s\omega/c$ is the sound source rotational Mach number. J' denotes the derivative of the Bessel function. $n = 1$ represents the incident pressure of BPF blade noise.

Multi-domain direct boundary element method (BEM) was employed to calculate the blade and casing noise radiation, i.e., to solve the inhomogeneous wave equations. The acoustic pressure and the normal velocity constitute the primary variables for the direct boundary element method. Continuity of acoustic pressure and the normal particle velocity is enforced at the interfaces of each sub-domain BEM model. Two BEM models with an identical mesh of the volute casing surface, one for the acoustic interior problem and the other for the exterior problem, were constructed; these two mesh models were coupled together at the openings, i.e. the inlet and outlet. The volute casing was modeled as a rigid structure to reflect incident waves such that the interior aerodynamic could only propagate outside through the casing inlet and outlet openings. According to the commonly applied rule of thumb, using six (linear) elements per wavelength [28], the maximum frequency, for which the discretization of the acoustic mesh is valid, is 2656 Hz; such that the mesh is fine enough to analyze the BPF 580 Hz noise.

Of the casing dipole source, since the acoustic BEM mesh of the casing was coarser than the CFD surface mesh, an interpolation of pressure from the CFD results to acoustic was carried out. Fast Fourier transform was performed to the pressure fluctuation time series to obtain the BPF component. Fig. 11 shows the BPF dipole source distribution on the casing interior surface. The area surrounding the volute tongue has the greatest value of acoustic source amplitude; this is because that the volute tongue is closest to the impeller such that the flow interaction between the impeller and the fixed volute tongue is the most vehement. The rest place of the casing surface which is near the impeller outlet also has intense dipole source ascribed to the strong interaction of the incoming unsteady air flow from the rotating impellor with the stationary casing.

Of the blade aerodynamic source, the blade was divided into 10 segments with the points of force application numbered, see Fig. 12. The representation of the fan blade noise by several Lawson's fan sources is a good approximation when the sizes of the blade segments are small compared to the wavelength (compact source approximation). The resulting radial, tangential and axial force components were obtained by integrating the pressure over each segment surface. By using Eq. (16) the incident pressure of BPF blade noise was obtained.

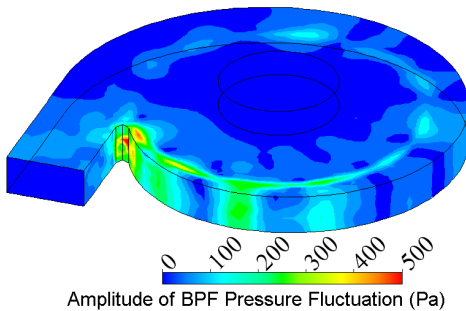


Fig. 11. Strength of BPF dipole source

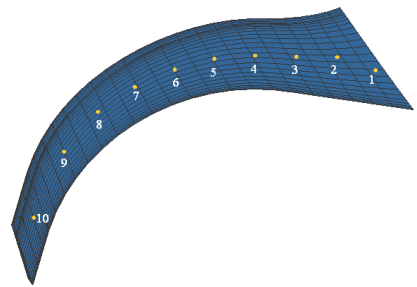


Fig. 12. Segments of blade surface

The casing was viewed as rigid in calculation of aerodynamic noise radiation, i.e., the normal velocity vanished on the casing surface; only the normal velocity at the inlet and outlet interfaces and the surface pressure on the whole BEM mesh needed to be solved. The surface pressure on the exterior BEM model is shown in Fig. 13. One can see that surface pressure of the casing noise is much higher than the blade noise.

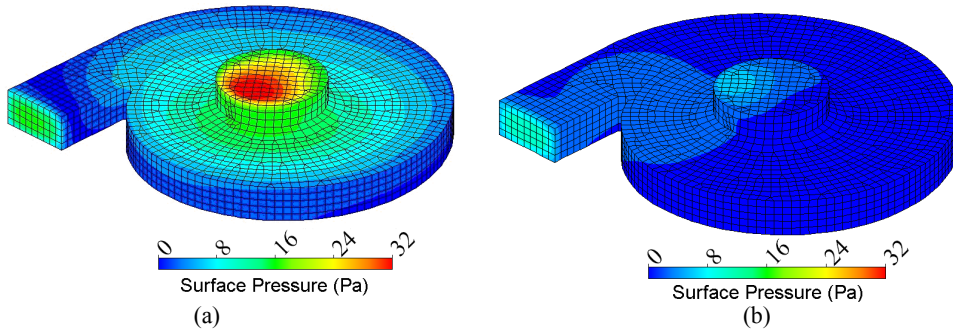


Fig. 13. Surface pressure distribution: (a) casing noise; (b) blade noise

A spherical field point mesh with the radius of 1 meter and centered at the geometric center of the volute casing was created outside the casing; the radiation field was evaluated at the field point mesh to obtain the radiated sound power. The sound power levels of casing and blade BPF aeroacoustic noise are 103 dB and 91 dB (ref. 10^{-12} W), respectively; the maximum sound pressure levels on the field point mesh are 97.6 dB and 86.9 dB (re 2×10^{-5} Pa), respectively.

Thus BPF aerodynamic noise generated by the casing dipole is much higher than the blade noise (over 10 dB). Locations around the impeller exit over the volute surface are the main noise sources due to the impeller-volute interaction, especially the volute tongue which is nearest to the impeller outlet.

Calculation of Casing Structural Noise

In studying the casing aeroacoustic noise at the previous section, the pressure fluctuation over the interior casing surface was modeled as surface dipole source, and the volute casing was regarded as rigid. As a matter of fact, the volute casing is an elastic structure, and under the excitation of aerodynamic pressure fluctuations it will vibrate; this vibration leads to structural noise radiation. In this section, the forced vibration and noise radiation of the volute casing structure was studied. The structural vibration was calculated using FEM and sound radiation was obtained by BEM.

Using FEM technique, structural dynamics can be depicted in a matrix form:

$$\mathbf{M}\ddot{\mathbf{u}}_s + \mathbf{C}\dot{\mathbf{u}}_s + \mathbf{K}\mathbf{u}_s = \mathbf{F} \quad (17)$$

where \mathbf{M} , \mathbf{C} and \mathbf{K} are structural mass, damping and stiffness matrix; the nodal acceleration, velocity and displacement vectors are $\ddot{\mathbf{u}}_s$, $\dot{\mathbf{u}}_s$ and \mathbf{u}_s , respectively, and the applied load vector is \mathbf{F} . To time harmonic excitations such as the BPF pressure fluctuations, the load vector has the form $\mathbf{F}e^{i\omega t}$ (where \mathbf{F} is a complex vector and $i = \sqrt{-1}$), thus the steady-state displacement response can be represented as $\mathbf{u}_s e^{i\omega t}$; with these expressions Eq. (17) can be written into:

$$(-\omega^2 \mathbf{M} + i\omega \mathbf{C} + \mathbf{K})\mathbf{u}_s = \mathbf{F} \quad (18)$$

Structural sound radiation at a specific frequency is governed by the frequency-domain wave equation, i.e., the Helmholtz equation:

$$\nabla^2 p' + k^2 p' = 0 \quad (19)$$

where k is wave number, defined as $k = \omega/c$. On the boundary of vibrating structures, the relationship between the normal acoustic pressure gradient of the fluid and the normal acceleration of the structure is given by:

$$\mathbf{n} \cdot \nabla p' = -\rho_0 \mathbf{n} \cdot \frac{\partial^2 \mathbf{u}_s}{\partial t^2} \quad (20)$$

where \mathbf{n} is the unit normal vector to the structure surface, and ρ_0 is the mean fluid density. After Fourier transform, it gives:

$$\mathbf{n} \cdot \nabla p' = \omega^2 \rho_0 \mathbf{n} \cdot \mathbf{u}_s \quad (21)$$

This is equivalent to give the second (Neumann) boundary condition to the Helmholtz equation. Eq. (20) can also be written as in frequency domain:

$$\partial p' / \partial n = -i\omega \rho_0 v_n \quad (22)$$

where v_n is the normal fluid velocity at the interface, which is equal to the normal structural velocity due to the velocity compatibility condition. The Sommerfeld radiation condition must be satisfied at the boundary surface located at infinity, in order to ensure that all acoustic waves propagate freely towards infinity and that no reflections occur at this boundary:

$$\lim_{r \rightarrow \infty} r \left(\frac{\partial p'}{\partial r} + ikp' \right) = 0 \quad (23)$$

Of the casing FEM model, a total of 34,896 shell elements were used in ANSYS[®] regarding that the casing is a thin shell structure. The shell element has six degrees of freedom at each node: translations in the nodal x , y , and z directions and rotations about the nodal x , y , and z axes. The material is steel, so the density $\rho = 7800 \text{ kg/m}^3$, Young's modulus $E = 2.0 \times 10^{11} \text{ Pa}$, and Poisson's ratio $\nu = 0.3$. The volute casing was fixed to the supporting stand by four fastening bolts at the casing backside. Three translational degrees of freedom of nodes at bolts were restricted to zero.

In order to validate the casing FEM model, modal analysis was performed firstly. Of the FEM model, totally 112 modes under 2000 Hz were extracted. Modal impact experiment was conducted on the casing. A total of 201 points on the volute casing surface were impacted by moving the hammer. Three accelerometers were placed at three fixed locations to measure the responses. Therefore, a total of 201×3 frequency response functions were obtained. Modal parameters (natural frequencies and damping) were estimated by the least squares complex exponential method [29]. The computed natural frequencies of first seven modes are compared with the measured ones in Table 1; a good agreement is found between the results of FEM and EMA (experimental modal analysis). Estimated damping ratios were about 0.5 % of the poles around BPF in the stabilization plots of modal analysis, therefore we took the damping ratio $\zeta = 0.005$ to account for all the damping effects in the calculation of the harmonic response.

Table 1. Natural frequencies of the casing structure

FEA (Hz)	51.1	62.0	90.3	118	142	187	199
EMA (Hz)	51.7	61.9	83.0	115	131	178	194
Relative error %	1.2	0.16	8.8	2.6	8.4	5.1	2.6

The amplitude of the casing normal vibration is shown in Fig. 14. The maximum normal velocity is 8.36 mm/s, i.e., the maximum displacement amplitude of the casing vibration is $|8.36/i\omega| = 0.00229 \text{ mm} = 2.29 \mu\text{m}$, which is at the order of magnitude of micrometer. The vibration pattern is rather complex: several locations with large amplitude distributed over the whole casing surface.

In this section, direct boundary element method (DBEM) was employed to calculate the sound radiation of the casing vibration. The BEM mesh and the field point mesh are the same as the previous section. As the surface mesh of DBEM acoustics must be closed, the inlet and outlet openings of the casing were blocked with elements. From the former structure FEA results, the casing normal vibration velocity v_n was known, and zero normal velocity boundary condition was imposed on the elements of inlet and outlet openings. Therefore, only the surface sound pressure p' should be solved. The radiated sound power by the casing vibration is $77.12 \mu\text{W}$ (i.e., 79 dB), and the maximum sound pressure on the field point mesh is 0.119 Pa

(75.5 dB). The sound pressure distribution on the field point mesh is shown in Fig. 15; owing to the complex vibration pattern, the sound directivity is quite complicated.

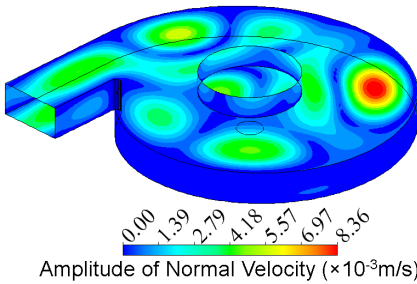


Fig. 14. Amplitude of casing structural vibration

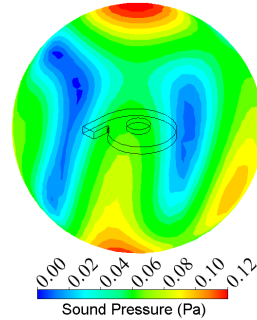


Fig. 15. Sound pressure distribution

Compared to the BPF aerodynamic noise, the structural noise is fairly small. The contributions of the BPF noise are listed in Table 2: the casing aerodynamic noise is largest contribution followed by the blade noise, and casing structural noise is the smallest contribution.

Table 2. Contributions of BPF fan noise

BPF noise contribution	Casing aerodynamic noise	Blade aerodynamic noise	Casing structural noise
Sound Power Level	103 dB	91 dB	79 dB
Maximum Sound Pressure	97.6 dB	86.9 dB	75.5 dB

Though the casing structural noise is negligible compared to the aerodynamic counterpart, the study of flow-induced casing vibration and sound radiation is very important. Because in many application cases, fans, pumps and compressors are installed in pipelines, the noise around these facilities are ascribed to structural vibration; the internal flow-induced noise radiates into the air via casing structural vibration. Casing vibration is excited by both the hydraulic pressure wave (fluctuation) and acoustic wave caused by rotor-stator interactions. The hydraulic and acoustic pressure waves have the same frequencies, while the amplitude of the latter is usually several orders smaller than that of the former. Because their frequencies are coincident, the influences of acoustics waves on structural vibration are negligible [30]. Therefore, in this study the casing vibration was calculated by inputting only the hydraulic pressure at the fluid-wall interface. The fluid-structure-sound weakly coupling methodology presented in this study is intended for studying flow-induced casing vibration and sound emission of turbo-machinery, especially for pumps and compressors.

Conclusions

In this paper, the blade passing frequency (BPF) noise contributions of a centrifugal fan, i.e., casing aerodynamic sound, blade aerodynamic sound and casing structural sound, were systematically studied. The 3-D unsteady flow field of the centrifugal fan was simulated by CFD. The casing and blade aeroacoustic dipole sources were extracted according to the acoustic analogy theory from the unsteady flow field, and the aerodynamic sound radiation was solved by BEM taking into account the scattering effect of the casing structure. The forced vibration of the volute casing under the excitation of pressure fluctuation at the fluid-wall interface was analyzed by FEM, and the structural sound radiation was calculated by BEM.

The flow field revealed the characteristics of impeller-volute flow interaction. Wakes exist at the blade suction side around the trailing edge. The circumferential non-uniform flow pattern at

the impeller outlet causes the regular pressure fluctuation on the downstream volute casing surface with the BPF as the fundamental frequency. The volute tongue which is closest to the rotating impeller among the whole volute surface constitutes the main aeroacoustic source. The blade suffers great pressure fluctuation as it sweeps over the volute tongue; however the BPF pressure fluctuation on the blade is not appreciable.

As for the noise contributions, the casing aerodynamic noise is predominant with the sound power level of 103 dB; the blade aerodynamic noise is 91 dB, and the casing structural noise is 79 dB. Therefore, in order to reduce the noise of this centrifugal fan, the aerodynamic noise should be abated, and the volute tongue being the main noise source is the primary target.

The study of flow-induced casing vibration and sound radiation is important, although the casing structural noise is negligible compared to the aerodynamic noise. The fluid-structure-sound one way coupling methodology presented in this study can be applied to various frequency noise caused by fan casing vibration. Moreover, its application can be extended to the forced casing vibration and sound emission of pumps and compressors, where sound emission is ascribed to structural and mechanical vibration.

Acknowledgements

This research is financially supported by the National Nature Science Foundation of China under Grant No. 50976084.

References

- [1] **Ballesteros-Tajadura R., Velarde-Suarez S., Hurtado-Cruz J. P.** Noise prediction of a centrifugal fan: numerical results and experimental validation. *Journal of Fluids Engineering*, Vol. 130, Issue 9, 2008, p. 1 – 12.
- [2] **Neise W.** Noise reduction in centrifugal fans: a literature survey. *Journal of Sound and Vibration*, Vol. 45, Issue 3, 1976, p. 375 – 403.
- [3] **Neise W.** Review of noise reduction methods for centrifugal fans. *Journal of Engineering for Industry*, Vol. 104, Issue 2, 1982, p. 151 – 161.
- [4] **Jeon W. H.** Overview of numerical analysis of fan noise. *Proceedings of Fan Noise 2003*, Senlis, France, 2003.
- [5] **Ballesteros-Tajadura R., Velarde-Suárez S., Hurtado-Cruz J., Santolaria-Morros C.** Numerical calculation of pressure fluctuations in the volute of a centrifugal fan. *Journal of Fluids Engineering*, Vol. 128, Issue 2, 2006, p. 359 – 369.
- [6] **Khelladi S., Kouidri S., Bakir F., Rey R.** Predicting tonal noise from a high rotational speed centrifugal fan. *Journal of Sound and Vibration*, Vol. 313, Issue 1-2, 2008, p. 113 – 133.
- [7] **Younsi M., Bakir F., Kouidri S., Rey R.** Numerical and experimental study of unsteady flow in a centrifugal fan. *Journal of Power and Energy*, Vol. 221, Issue 7, 2007, p. 1025 – 1036.
- [8] **Wang M., Freund J., Lele S. K.** Computational prediction of flow-generated sound. *Annual Review of Fluid Mechanics*, Vol. 38, 2006, p. 483 – 512.
- [9] **Diaz K. M. A., Oro J. M. F., Marigorta E. B., Morros C. S.** Numerical prediction of tonal noise generation in an inlet vaned low-speed axial fan using a hybrid aeroacoustic approach. *Journal of Mechanical Engineering Science*, Vol. 223, Issue 9, 2009, p. 2081 – 2098.
- [10] **Bailly C., Bogey C., Gloerfelt X.** Some useful hybrid approaches for predicting aerodynamic noise. *Comptes Rendus Mécanique*, Vol. 333, Issue 9, 2005, p. 666 – 675.
- [11] **Lele S. K.** Computational aeroacoustics – a review. *AIAA, 35th Aerospace Sciences Meeting & Exhibit*, Reno, NV, USA, 1997.
- [12] **Lighthill M.** On sound generated aerodynamically. I. General theory. *Proceedings of the Royal Society of London, Series A, Mathematical and Physical Sciences*, Vol. 211, Issue 1107, 1952, p. 564 – 587.
- [13] **Ffowcs Williams J., Hawkings D.** Sound generation by turbulence and surfaces in arbitrary motion. *Royal Society of London Philosophical Transactions, Series A*, Vol. 264, Issue 1151, 1969, p. 321 – 342.

- [14] **Gloerfelt X., Bailly C., Juvé D.** Direct computation of the noise radiated by a subsonic cavity flow and application of integral methods. *Journal of Sound and Vibration*, Vol. 266, Issue 1, 2003, p. 119 – 146.
- [15] **Lin S.-C., Tsai M.-L.** An integrated performance analysis for a backward-inclined centrifugal fan. *Computers & Fluids*, Vol. 56, Issue 3, p. 24 – 38.
- [16] **Liu Q., Qi D., Tang H.** Computation of aerodynamic noise of centrifugal fan using large eddy simulation approach, acoustic analogy, and vortex sound theory. *Journal of Mechanical Engineering Science*, Vol. 221, Issue 11, 2007, p. 1321 – 1332.
- [17] **Langthjem M. A., Olhoff N.** A numerical study of flow-induced noise in a two-dimensional centrifugal pump. Part II. Hydroacoustics. *Journal of Fluids and Structures*, Vol. 19, Issue 3, 2004, p. 369 – 386.
- [18] **Jeon W. H., Lee D. J.** An analysis of the flow and aerodynamic acoustics sources of a centrifugal impeller. *Journal of Sound and Vibration*, Vol. 222, Issue 3, 1999, p. 505 – 511.
- [19] **Neise W.** Review of fan noise generation mechanisms and control methods. *Proceedings of Fan Noise 1992*, Senlis, France, 1992.
- [20] **Qi D., Mao Y., Liu X., Yuan M.** Experimental study on the noise reduction of an industrial forward-curved blades centrifugal fan. *Applied Acoustics*, Vol. 70, Issue 8, 2009, p. 1041 – 1050.
- [21] **Versteeg H. K., Malalasekera W.** An introduction to computational fluid dynamics. The finite volume method. Essex, U. K.: Longman Scientific & Technical Publishing, 1995.
- [22] **Ayar A., Ambs R., Capellmann C., Schillemeit B., Matthes M.** Prediction of flow-induced noise in automotive HVAC systems using a combined CFD/CA approach. *SAE Transactions*, Vol. 114, Issue 6, 2005, p. 550 – 564.
- [23] **Reese H., Carolus T., Kato C.** Numerical prediction of the aeroacoustic sound sources in a low pressure axial fan with inflow distortion. *Proceedings of Fan Noise 2007*, Senlis, France, 2007.
- [24] **Khelladi S., Kouidri S., Bakir F., Rey R.** Flow study in the impeller-diffuser interface of a vaned centrifugal fan. *Journal of Fluids Engineering*, Vol. 127, Issue 3, 2005, p. 495 – 502.
- [25] **Cai J. C.** A Study on the Generation and Propagation of the Blade Passing Frequency Noise of a Centrifugal Fan. Xi'an, China: Ph. D. Thesis, Xi'an Jiao Tong University, 2011.
- [26] **Lakshminarayana B.** Fluid Dynamics and Heat Transfer of Turbomachinery. New York, U. S.: John Wiley & Sons, Inc., 1996.
- [27] **Curle N.** The influence of solid boundaries upon aerodynamic sound. *Proceedings of the Royal Society of London, Series A, Mathematical and Physical Sciences*, Vol. 231, Issue 1187, 1955, p. 505 – 514.
- [28] **Marburg S.** Six boundary elements per wavelength: is that enough? *Journal of Computational Acoustics*, Vol. 10, Issue 1, 2002, p. 25 – 52.
- [29] **Ewins D. J.** Modal Testing: Theory, Practice and Application. Hertfordshire, U. K.: Research Studies Press, Ltd., 2000.
- [30] **Jiang Y., Yoshimura S., Imai R., Katsura H., Yoshida T., Kato C.** Quantitative evaluation of flow-induced structural vibration and noise in turbomachinery by full-scale weakly coupled simulation. *Journal of Fluids and Structures*, Vol. 23, Issue 4, 2007, p. 531 – 544.